Possible coexistence of principal and tilted axis rotation in ^{103}Ag

P. Datta, S. Chattopadhyay, P. Banerjee, S. Bhattacharya, J. Chatterjee, B. Dasmahapatra, C. C. Dey, T. K. Ghosh, A. Goswami, S. Pal, I. Ray, M. Saha Sarkar, and S. Sen
Saha Institute of Nuclear Physics, 1/AF Bidhan Nagar, Kolkata 700 064, India

H. C. Jain and P. K. Joshi
Tata Institute of Fundamental Research, Homi Bhabha Road, Mumbai 400 005, India

Amita
Department of Physics, RBS College, Agra 282 002, India
(Received 26 June 2002; published 31 January 2003)

The high spin states of ^{103}Ag have been populated through the ^{76}Ge(^{35}Cl, $\alpha 4n\gamma$)^{103}Ag reaction using 132-MeV ^{35}Cl beam. The presence of a positive parity ground state band and two negative parity bands decaying predominantly by $M1$ transitions in ^{103}Ag has been confirmed. In addition, seven new crossover $E2$ transitions have been observed in the negative parity bands. The experimental $B(M1)/B(E2)$ ratios are compared with the values obtained from the Dönau geometric formula for the negative parity bands based on single particle configurations assigned from signature arguments. These ratios are also compared to those obtained from the hybrid version of tilted axis cranking. A systematic study of odd-Ag isotopes seems to indicate that the signature symmetry is retained in ^{103}Ag due to the shallow tilted minimum.

DOI: 10.1103/PhysRevC.67.014325 PACS number(s): 27.60.+j, 21.10.Hw, 21.60.Ev

I. INTRODUCTION

In recent years, several bands decaying predominantly by $M1$ transitions [1] have been reported in $47 \leqslant Z \leqslant 50$ and $N > 50$ mass range with $B(M1)/B(E2)$ ratio varying between 10 and 50 $(\mu_N/e\,\mathrm{b})^2$. The theoretical explanation for this observation has been provided by the tilted axis cranking (TAC) [2,3] model. This model predicts a nonprincipal axis rotation in nuclei with small deformation where a deformation-coupled quasiproton (quasineutron) couples to a high-j rotation-coupled quasineutron (quasiproton) and the angular momentum is generated by gradual alignment of spins of the quasiparticles in the direction of the total angular momentum. It is to be noted that the signature symmetry is violated due to nonprincipal axis rotation and a regular increase in the $M1$ transition energies is predicted by the model.

However, similar bands in ^{102,104}Cd have been reported to exhibit staggering in $M1$ transition energies [4,5] which is in contrast to a regular increase as observed in other $M1$ bands [1,6]. Such energy staggering is generally associated with signature splitting which can only be accommodated in the framework of principal axis cranking. In the previous study of ^{103}Ag by Treherne *et al.* [7], two negative parity $M1$ bands were reported—one of them exhibits a regular increase in $M1$ transition energy with increasing spin while the other band shows an energy staggering. Furthermore, the states of same spins in these two bands are separated by $\sim$100 keV only. In the present work, ^{103}Ag has been revisited with the objective to investigate the structures of these two negative parity bands.

II. EXPERIMENT

^{103}Ag was produced at high angular momentum through ^{76}Ge(^{35}Cl, $\alpha 4n\gamma$)^{103}Ag reaction using 132-MeV ^{35}Cl beam from the 14-UD Pelletron at TIFR. The target was prepared by evaporating $\sim$700 μg/cm^2 of 99.8% enriched ^{76}Ge on a 10 mg/cm^2 thick Au foil. γ rays were detected by an array consisting of eight Compton suppressed Clover detectors [8]. Each Clover detector, in the addback mode, has 35% more photopeak efficiency around 1 MeV compared to that of four standard 110 cm^3 HPGe crystal. Detectors were placed at 60°, 90°, 120°, 150°, 215°, 255°, 285°, and 325° with respect to the beam direction. The directional correlation orientation (DCO) ratios of the γ rays were obtained from the following definition:

$$R_{\mathrm{DCO}} = \frac{I_\gamma(\text{observed at } 150°,\ 215°,\ \text{and } 325°,\ \text{gate on } 90°,\ 255°,\ \text{and } 285°)}{I_\gamma(\text{observed at } 90°,\ 255°,\ \text{and } 285°,\ \text{gate on } 150°,\ 215°,\ \text{and } 325°)}. \quad (1)$$

Altogether 200×10^6 threefold coincidences were collected. Two E_γ-E_γ matrices were formed by unfolding each threefold coincidence event into three twofold events with a time gate of 100 ns. The conventional symmetrized matrix was used to generate the background subtracted gated spectra, while the asymmetric matrix was used for extracting the

 ©2003 The American Physical Society

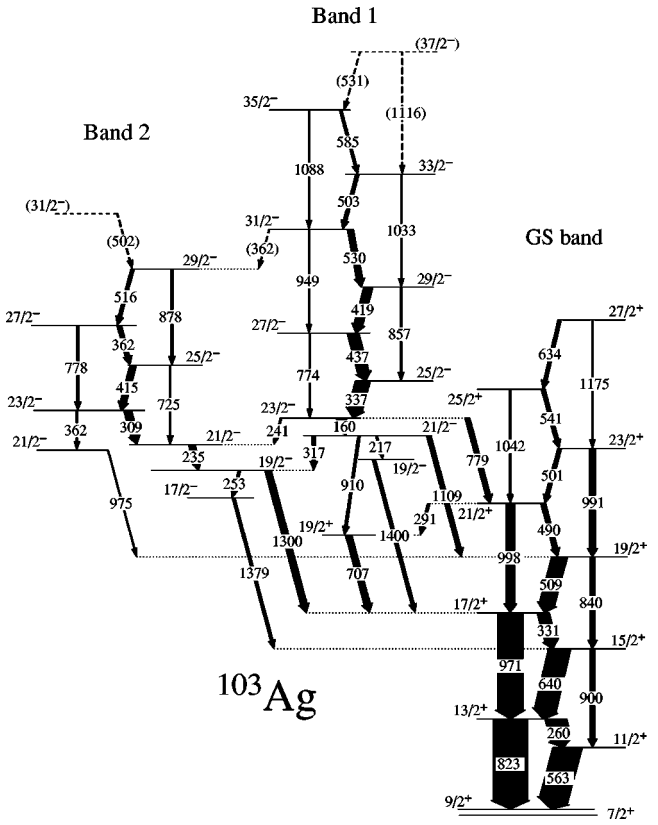

FIG. 1. Partial level scheme of ^{103}Ag. The γ transition energies are in keV.

DCO ratios. These matrices were analyzed using ESCL8R, SLICE, and GF3 programs of RADWARE [9].

III. RESULTS

The partial level scheme for ^{103}Ag is shown in Fig. 1, which was constructed from the symmetrized E_γ-E_γ matrix. Care was taken to avoid contaminations from other strong reaction channels present in the ^{35}Cl+^{76}Ge reaction. The intensities and the DCO ratios of the γ rays were extracted from the spectra generated with gates on the 235-, 337-, and 823-keV transitions. The values obtained are listed in Table I. The positive parity ground state (GS) band has been found to be in good agreement with the level scheme given by Treherne *et al.* [7]. The parities of bands 1 and 2 were determined in the previous work through the linear polarization measurement [7]. Besides the reconfirmation of $M1$ transitions reported earlier, four new crossover $E2$ transitions with energies 774, 949, 1033, and 1088 keV have been identified in band 1. These transitions are shown in the 337- and 823-keV gated spectra (Fig. 2). The spectra with gates on $M1$ transitions in band 2 show a 502-keV γ transition, which has been tentatively placed above the $29/2^-$ level. In addition, three weak crossover $E2$ transitions have also been identified in band 2. In a significant modification of the earlier level scheme, the positions of 362- and 415-keV transitions have been interchanged in band 2. This was suggested from the observation that the intensity of the 362-keV γ ray is comparable to that of the 415-keV γ ray in the 823-keV ($13/2^+$ to $9/2^+$) gate. But the 362-keV gated γ spectrum shows a 362-keV γ peak presumably due to the 362-keV transition deexciting the $23/2^-$ state in band 2. This transition was reported by Treherne *et al.* [7]. Thus, the intensity of each of the 362-keV transition is smaller than the intensity of the 415-keV γ ray and justifies the proposed interchange (Table I). This was further supported by the observation of the new crossover $E2$ transitions with energies of 725 and 878 keV as shown in spectra with 235- and 823-keV gates (Fig. 2). It should be further noted that the intensities of the 362-keV and the 415-keV γ rays are comparable even in the 235-keV gated spectrum (Fig. 2), which excludes the second 362-keV ($23/2^+$ to $21/2^+$) transition. In addition, the 975-keV transition (band 2) deexciting the $21/2^-$ level (which is fed by the second 362-keV transition) has an intensity of 3.5 ± 0.3. This is much smaller compared to 6.8 ± 0.6, which is the self-gated intensity of the 362-keV transition. Both of these observations support the possibility of a third 362-keV transition which is in coincidence with the 235- and 362-keV γ rays. Therefore, a third 362-keV transition has been tentatively placed between the $31/2^-$ level of band 1 and $29/2^-$ level of band 2. However, no other interband transitions have been found between bands 1 and 2.

IV. DISCUSSIONS

The band structure in ^{103}Ag is governed by the $g_{9/2}$ proton orbital and $d_{5/2}$, $g_{7/2}$, and $h_{11/2}$ neutron orbitals. The positive parity ground state band in ^{103}Ag has been reasonably well understood within the framework of the particle rotor model with variable moment of inertia [7,10]. In this model, the $\pi(g_{9/2})^{-1}$ hole is coupled to an axial rotor core of ^{104}Cd. A negative parity band with large band head spin, on the other hand, can originate only from the excitation of one neutron to $h_{11/2}$ orbital, from $d_{5/2}$ or $g_{7/2}$ orbitals since it is quite improbable to excite the last proton to the $h_{11/2}$ orbital across the large $N=50$ shell gap. This is shown in Fig. 3 where the single particle orbitals for this mass range have been plotted as a function of quadrupole deformation (ϵ_2). It is also observed from this figure that the $\Omega=3/2$ of $d_{5/2}$ and $\Omega=1/2$ of $g_{7/2}$ orbitals cross each other at around $\epsilon_2=0.13$. Therefore, at this deformation, the last pair of the 56 neutrons in ^{103}Ag can occupy either of these two orbitals. In a previous calculation, Crowell *et al.* [11] reported a quadrupole deformation of 0.14 for the above-mentioned configuration in ^{103}Ag. Thus, if bands 1 and 2 originate due to neutron excitation from $\Omega=3/2$ of $d_{5/2}$ and $\Omega=1/2$ of $g_{7/2}$, then the band head energies are expected to be very close to each other. In addition, as the high-j configurations of the two $M1$ bands are same (viz., $\pi g_{9/2}\otimes\nu h_{11/2}$), the gross behaviors of bands 1 and 2, are expected to be similar.

Even though the similarity in configurations has been emphasized above, a closer look shows very distinct properties for both the negative parity bands. This is shown in Figs. 4 and 5 where the $B(M1)/B(E2)$ ratios and the level energy differences $E(I)-E(I-1)$ are plotted as a function of angular momentum. It is evident from Fig. 4 that both the bands have large values of $B(M1)/B(E2)$ ratios but the values for band 1 are twice as large as those of band 2 at all spins. It is

TABLE I. Relative intensities, DCO ratios, and γ energies E_γ for transitions deexciting energy levels E_i in ^{103}Ag. Unless otherwise mentioned, the values in columns 5 and 6 are obtained from gates on the pure 235-keV dipole (D) transition and 823-keV pure quadrupole (Q) transition, respectively.

E_γ (keV)	E_i (keV)	$I_i^\pi \rightarrow I_f^\pi$	Relative intensity	R_{DCO}(D)	R_{DCO}(Q)
160	3599	$23/2^- \rightarrow 21/2^-$	28.0(1.2)		0.54(0.09)[a]
217	3339	$21/2^- \rightarrow 19/2^-$	6.0(0.4)		
235	3357	$21/2^- \rightarrow 19/2^-$	19.0(0.7)		0.56(0.09)[a]
241	3599	$23/2^- \rightarrow 21/2^-$	5.5(0.5)		
253	3122	$19/2^- \rightarrow 17/2^-$	7.9(0.6)	1.06(0.16)	
260	851	$13/2^+ \rightarrow 11/2^+$	63.0(2.1)	0.92(0.12)	
291	2830	$21/2^+ \rightarrow 19/2^-$	8.0(0.5)		
309	3667	$23/2^- \rightarrow 21/2^-$	23.0(1.0)	1.00(0.10)	
317	3439	$21/2^- \rightarrow 19/2^-$	9.2(0.5)		
331	1830	$17/2^+ \rightarrow 15/2^+$	36.0(1.2)	0.96(0.14)	0.67(0.08)
337	3936	$25/2^- \rightarrow 23/2^-$	44.0(1.6)		0.65(0.07)[a]
362	3667	$23/2^- \rightarrow 21/2^-$	3.5(0.3)		
362	4444	$27/2^- \rightarrow 25/2^-$	13.7(1.0)	0.93(0.11)	
362	5322	$31/2^- \rightarrow 29/2^-$	3.3(0.5)		
415	4082	$25/2^- \rightarrow 23/2^-$	19.5(1.0)	0.93(0.14)	
419	4793	$29/2^- \rightarrow 27/2^-$	27.0(0.7)		0.68(0.10)
437	4373	$27/2^- \rightarrow 25/2^-$	35.0(0.7)		0.70(0.11)[a]
490	2820	$21/2^+ \rightarrow 19/2^+$	15.0(0.8)		0.60(0.10)[a]
501	3321	$23/2^+ \rightarrow 21/2^+$	12.0(0.7)		0.75(0.13)
503	5825	$33/2^- \rightarrow 31/2^-$	10.5(0.5)		0.71(0.12)
509	2330	$19/2^+ \rightarrow 17/2^+$	47.0(1.3)		
516	4960	$29/2^- \rightarrow 27/2^-$	10.4(0.5)	0.95(0.16)	
530	5323	$31/2^- \rightarrow 29/2^-$	19.0(0.8)		0.67(0.10)
541	3862	$25/2^+ \rightarrow 23/2^+$	11.8(1.0)		0.60(0.10)
563	591	$11/2^+ \rightarrow 9/2^+$	87.0(3.4)	1.07(0.14)	
585	6411	$35/2^- \rightarrow 33/2^-$	8.0(0.5)		
634	4496	$27/2^+ \rightarrow 25/2^+$	10.6(0.7)		
640	1491	$15/2^+ \rightarrow 13/2^+$	67.0(2.0)	0.89(0.15)	
707	2529	$19/2^- \rightarrow 17/2^+$	19.5(0.9)		0.64(0.11)
725	4082	$25/2^- \rightarrow 21/2^-$	4.6(0.3)		
774	4373	$27/2^- \rightarrow 23/2^-$	3.0(0.2)		
778	4444	$27/2^- \rightarrow 23/2^-$	6.3(0.4)		
779	3599	$23/2^- \rightarrow 21/2^+$	15.0(1.2)		1.08(0.16)
823	851	$13/2^+ \rightarrow 9/2^+$	104.0(4.1)	1.52(0.21)	1.00(0.11)[a]
840	2230	$19/2^+ \rightarrow 15/2^+$	15.4(1.0)		
857	4793	$29/2^- \rightarrow 25/2^-$	5.0(0.3)		
878	4960	$29/2^- \rightarrow 25/2^-$	6.3(0.4)		
900	1491	$15/2^+ \rightarrow 11/2^+$	15.0(1.0)		
910	3439	$21/2^- \rightarrow 19/2^-$	7.5(0.6)		
949	5323	$31/2^- \rightarrow 27/2^-$	3.2(0.3)		
971	1822	$17/2^+ \rightarrow 13/2^+$	77.0(3.0)	1.56(0.24)	1.07(0.12)
975	3304	$21/2^- \rightarrow 19/2^+$	3.5(0.3)		
991	3321	$23/2^+ \rightarrow 19/2^+$	15.8(0.8)		
998	2820	$21/2^+ \rightarrow 17/2^+$	26.0(1.1)		
1033	5825	$33/2^- \rightarrow 29/2^-$	3.3(0.2)		
1042	3862	$25/2^+ \rightarrow 21/2^+$	5.0(0.7)		
1088	6411	$35/2^- \rightarrow 31/2^-$	3.6(0.3)		
1109	3439	$21/2^- \rightarrow 19/2^+$	14.0(0.8)		
1300	3122	$19/2^- \rightarrow 17/2^+$	20.0(0.9)	0.91(0.12)	0.58(0.10)

TABLE I. (*Continued*.)

E_γ (keV)	E_i (keV)	$I_i^\pi \rightarrow I_f^\pi$	Relative intensity	$R_{\rm DCO}$(D)	$R_{\rm DCO}$(Q)
1379	2869	$17/2^- \rightarrow 15/2^+$	8.8(0.6)		
1400	3222	$19/2^- \rightarrow 17/2^+$	10.3(0.7)		

[a] $R_{\rm DCO}$ from gate on 971-keV transition.

also observed from Fig. 5 that both the bands exhibit a staggering in the $M1$ transition energies, but the phase of staggering is opposite. It should be recalled that the staggering appeared due to an interchange in positions of 415- and 362-keV transitions in band 2. This observation has been used to assign specific configurations to bands 1 and 2 as discussed below.

The favored signature for a single particle configuration is defined by [12]

$$\alpha_f = 1/2 \sum_i (-1)^{j_i - 1/2}, \tag{2}$$

where the summation runs over all unpaired neutrons and protons. Thus, the favored signature for the $\pi g_{9/2} \otimes \nu d_{5/2} \otimes \nu h_{11/2}$ configuration is $\alpha_f = 1/2$ and that for $\pi g_{9/2} \otimes \nu g_{7/2} \otimes \nu h_{11/2}$ configuration is $-1/2$. This explains the observation that the phase of staggering is opposite in the two bands. Therefore, from the signature argument, the configuration for band 1 can be suggested to be $\pi g_{9/2} \otimes \nu d_{5/2} \otimes \nu h_{11/2}$, while that for band 2 to be $\pi g_{9/2} \otimes \nu g_{7/2} \otimes \nu h_{11/2}$. It may be noted that the $\alpha_f = 1/2$ negative parity band in ^{101}Ag had also been assigned [13] the configuration of $\pi g_{9/2} \otimes \nu d_{5/2} \otimes \nu h_{11/2}$ by comparing the experimental level energies and electromagnetic transitions with the calculated values from the interacting boson fermion plus broken pair model.

As pointed out earlier, similar $M1$ bands $[B(M1)/B(E2) \sim 30(\mu_N/e\ \mathrm{b})^2]$ with staggering in $M1$ transition energy, have been observed in this mass region. The configurations for these bands can also be assigned through similar signature arguments. For example, the positive parity band 2 of ^{104}Cd [4] was proposed to originate from $\pi g_{9/2}^{-2} \otimes \nu h_{11/2}^2$ configuration for which the favored signature is $\alpha_f = 0$. It is indeed observed from the level scheme that even spin states are lower in energy.

In order to further establish the configurations for bands 1 and 2, the $B(M1)$ transition rates were estimated with the geometric formula by Dönau [14]. This model assumes a fixed K value and the alignments are perpendicular to the symmetry axis. $B(M1)$ values for bands with no signature splitting are given by

$$B(M1) = \frac{3}{8\pi} \frac{K^2}{I^2} [(g^{(1)} - g_R)(\sqrt{I^2 - k^2} - i_x^{(1)}) - (g^{(2)} - g_R) i_x^{(2)}]^2, \tag{3}$$

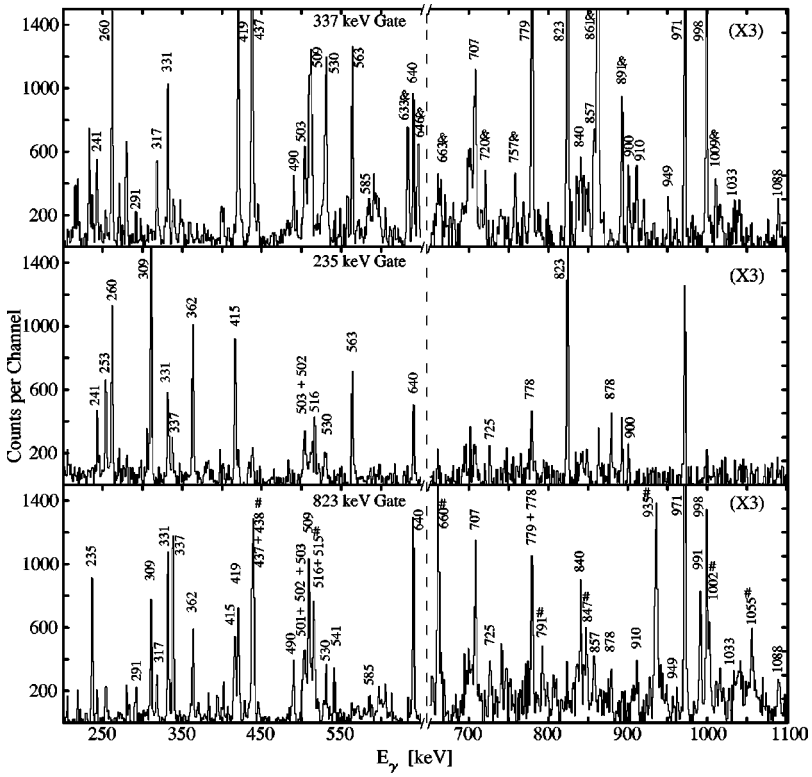

FIG. 2. γ-γ coincidence spectra with 823-, 235-, and 337-keV gates in ^{76}Ge(^{35}Cl, $\alpha 4n\gamma$)^{103}Ag reaction. The counts beyond 650 keV have been scaled up by a factor of 3. The contaminant γ transitions from ^{107}In and ^{106}Cd have been marked by # and &, respectively.

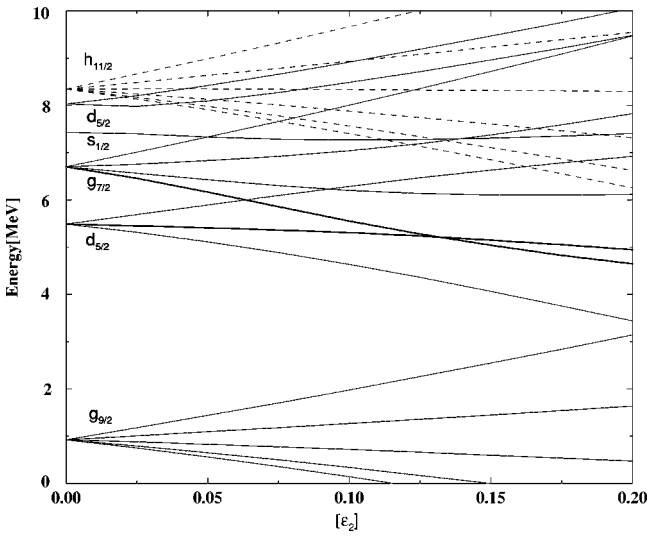

FIG. 3. The single particle levels in a deformed Woods-Saxon potential for ^{103}Ag as a function of quadrupole deformation ϵ_2 [16]. The $\Omega=3/2$ of $d_{5/2}$ and $\Omega=1/2$ of $g_{7/2}$ levels have been highlighted.

where the superscripts (1) and (2) refer to the deformation-aligned and rotation-aligned configurations, respectively [15]. The rotational aligned g factor ($g^{(2)}$) is calculated from

$$g^{(2)}K^{(2)}=g_{\Omega_1}\Omega_1+g_{\Omega_2}\Omega_2 \tag{4}$$

and

$$K^{(2)}=\Omega_1+\Omega_2, \tag{5}$$

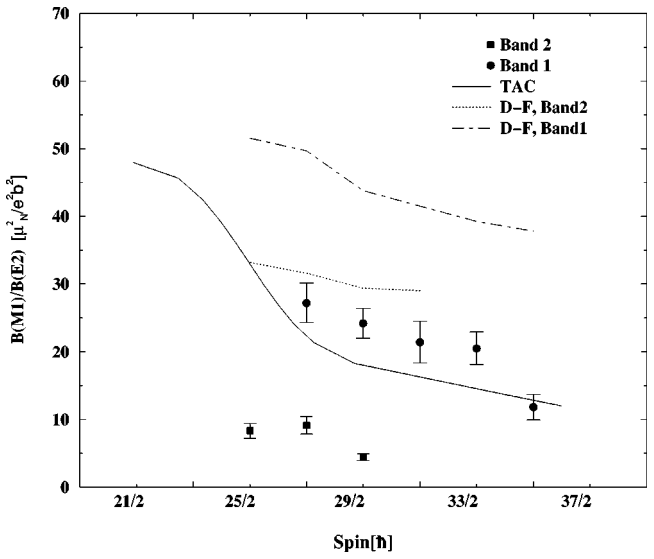

FIG. 4. Observed $B(M1)/B(E2)$ values as a function of angular momentum in the two negative parity bands of ^{103}Ag. The dotted and dot-dashed lines represent the calculated values from the geometric formula by Dönau and Frauendrof (DF) for $\pi g_{9/2}\otimes\nu g_{7/2}\otimes\nu h_{11/2}$ (band 2) and $\pi g_{9/2}\otimes\nu d_{5/2}\otimes\nu h_{11/2}$ (band 1) configurations, respectively. The solid line represents the calculated values from the TAC calculations at $\theta=70°$.

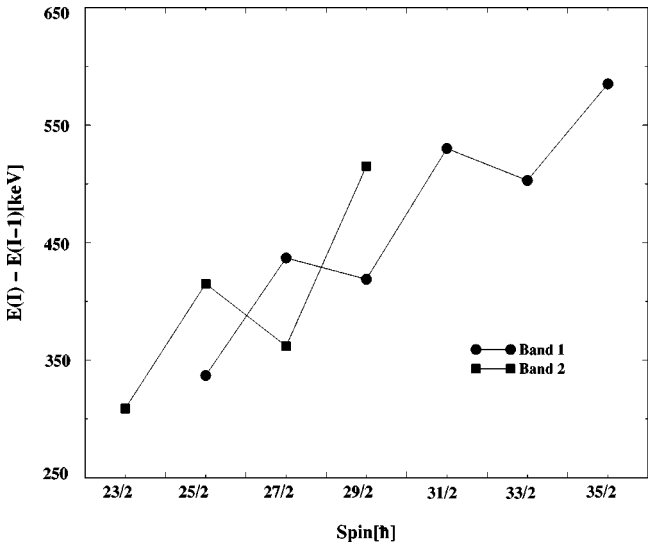

FIG. 5. Observed energy differences $E(I)-E(I-1)$ as a function of angular momentum (I) in two negative parity bands of ^{103}Ag.

where Ω_1 and Ω_2 are $\frac{1}{2}$ and $\frac{3}{2}$ for band 1 and $\frac{1}{2}$ and $\frac{1}{2}$ for band 2, respectively. The $g^{(2)}$ values, in the present case, were estimated by assuming $g(\nu h_{11/2})=-0.21$, $g(\nu d_{5/2})=-0.33$, and $g(\nu g_{7/2})=0.21$ [16]. The rotational g factor (g_R) was assumed to be Z/A.

The effect of signature splitting is incorporated in this model by multiplying the unfavored signature sequence by $(1-\Delta e/\omega)$ where Δe is the difference in the values of the experimental Routhians for the two signature sequences [17]. In the case of bands 1 and 2, the value of Δe is very close to zero because the observed signature splitting is very small. Thus, the correction due to signature splitting has been neglected for the calculation of the $B(M1)$ rates in bands 1 and 2.

The $B(E2)$ values are given by

$$B(E2,I\rightarrow I-2)=\frac{5}{16\pi}\frac{3(I-K)(I-K-1)(I+K)(I+K-1)}{(2I-2)(2I-1)I(2I+1)}Q_0^2, \tag{6}$$

where I is the initial spin and K is the projection of angular momentum on the symmetry axis [15].

Various parameters used to calculate the $B(M1)$ rates for both the configurations mentioned above are listed in Table II. The value of $i_x^{(1)}$ was extracted from the alignment value of the GS band. The reference parameters for the aligned angular momentum were assumed to be $\Im_0=7.0\hbar^2/\mathrm{MeV}$ and $\Im_1=15.0\hbar^4/\mathrm{MeV}^3$ [15]. The values of $i_x^{(2)}$ were estimated by subtracting $i_x^{(1)}$ from the alignment values of bands 1 and 2.

The $B(M1)/B(E2)$ values were calculated for $Q_0=1.5$ e b corresponding to $\epsilon_2\sim0.13$. The values obtained for bands 1 and 2 are shown in Fig. 4 by the dot-dashed and dotted lines, respectively. It is observed from this figure that the calculated ratios are higher than the experimental values.

TABLE II. Parameters used in the calculation of $B(M1)$ transition rates.

Band	K	DAL configuration	$i_x^{(1)}(\hbar)$	$g^{(1)}$	RAL configuration	$i_x^{(2)}(\hbar)$	$g^{(2)}$
1	$\frac{9}{2}$	$\pi[413]\frac{7}{2}^+$	1.5	+1.27	$\left(\nu[550]\frac{1}{2}^- \otimes \nu[422]\frac{3}{2}^+\right)$	6.5	−0.39
2	$\frac{9}{2}$	$\pi[413]\frac{7}{2}^+$	1.5	+1.27	$\left(\nu[550]\frac{1}{2}^- \otimes \nu[420]\frac{1}{2}^+\right)$	6.5	0

However, the calculated values for band 1 are clearly larger than those for band 2, which is in agreement with the experimental observation. This is primarily due to the fact that $g^{(2)}=-0.39$ for band 1, while it is zero for band 2. These calculations are reasonably insensitive to values of $i_x^{(2)}$. If the value of $i_x^{(2)}$ for band 2 is changed from $6.5\hbar$ to $8\hbar$, then the $B(M1)$ values change by 10%. Therefore, the opposite phase of the staggering in $M1$ transition energies and the larger values of $B(M1)/B(E2)$ ratios for band 1 are well understood by assuming $\pi g_{9/2}\otimes \nu d_{5/2}\otimes \nu h_{11/2}$ configuration for band 1 and $\pi g_{9/2}\otimes \nu g_{7/2}\otimes \nu h_{11/2}$ configuration for band 2.

In order to explore this situation further, the $B(M1)/B(E2)$ ratios were also calculated within the framework of the hybrid version of the TAC [18]. In this model, the spherical part of the single particle energies is taken from the spherical Woods-Saxon potential and combined with the deformed part of the anisotropic harmonic oscillator potential. This approximation has the advantage of using a realistic flat bottom potential. In addition, the coupling between the oscillator shells is taken into account in a simple way. In accordance with the previous discussion, the $\pi g_{9/2} \otimes \nu(g_{7/2}d_{5/2})^1\otimes \nu h_{11/2}$ configuration has been chosen for our calculations. It is to be noted that the two configurations, viz., $\pi g_{9/2}\otimes \nu d_{5/2}\otimes \nu h_{11/2}$ and $\pi g_{9/2}\otimes \nu g_{7/2}\otimes \nu h_{11/2}$, cannot be treated separately in the present model, as Ω is not a good quantum number in the TAC whereas parity remains conserved. The gap parameter Δ was chosen as 80% of the odd-even mass difference Δ_{oe} for protons and neutrons. The Δ_{oe} was calculated using the expressions given in Ref. [19] with the binding energies taken from the atomic mass table [20]. The chemical potential (λ) was properly chosen to reproduce the correct particle number. The equilibrium tilt angle (θ_0) was calculated by using the condition that the expectation values of the total angular momentum and angular velocity are parallel [21]. That is

$$\tan(\theta_0)=\frac{\omega_1}{\omega_3}=\frac{J_1}{J_3}, \tag{7}$$

where J_1 and J_3 are the components of total angular momentum I along the 1 axis and 3 axis, respectively. Its value was found to be 70° for ^{103}Ag at $\hbar\omega=0.3$ MeV. The equilibrium values for the deformation parameter ϵ_2 and γ were obtained by minimizing total Routhian with respect to the deformation

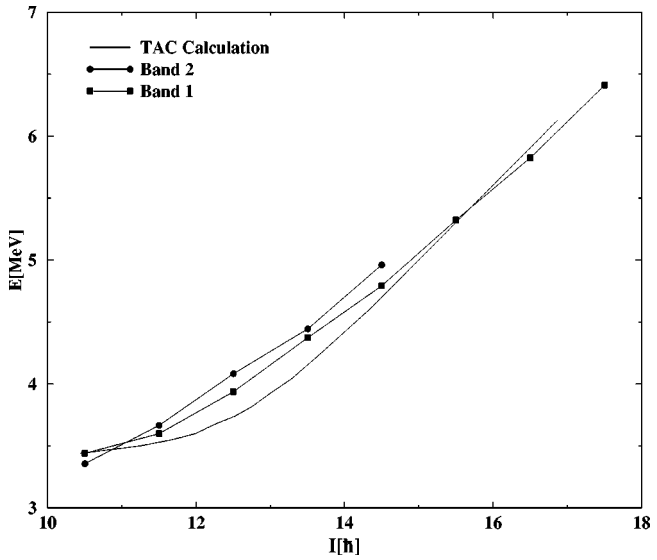

FIG. 6. Level energies E vs the total angular momentum I for ^{103}Ag. Rectangles and circles are the experimental data for bands 1 and 2, respectively. The solid line represents the calculated values which have been normalized at $I=21/2\hbar$. The experimental frequency is extracted from the measured γ energies using the relation $\hbar\omega(I)=E_\gamma=E(I)-E(I-1)$.

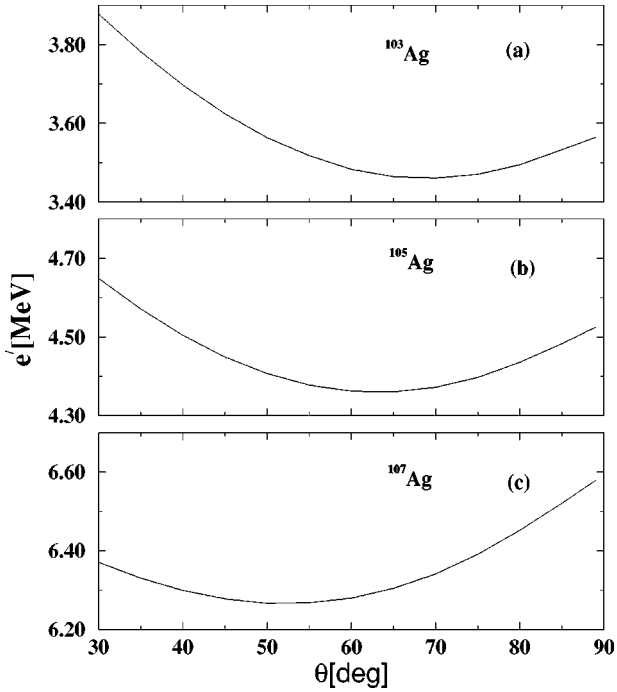

FIG. 7. The total quasiparticle Routhians at $\hbar\omega=0.3$ MeV for (a) ^{103}Ag, (b) ^{105}Ag, and (c) ^{107}Ag as a function of tilt angle for $\pi g_{9/2}\otimes \nu(g_{7/2}d_{5/2})^1\otimes \nu h_{11/2}$ configuration.

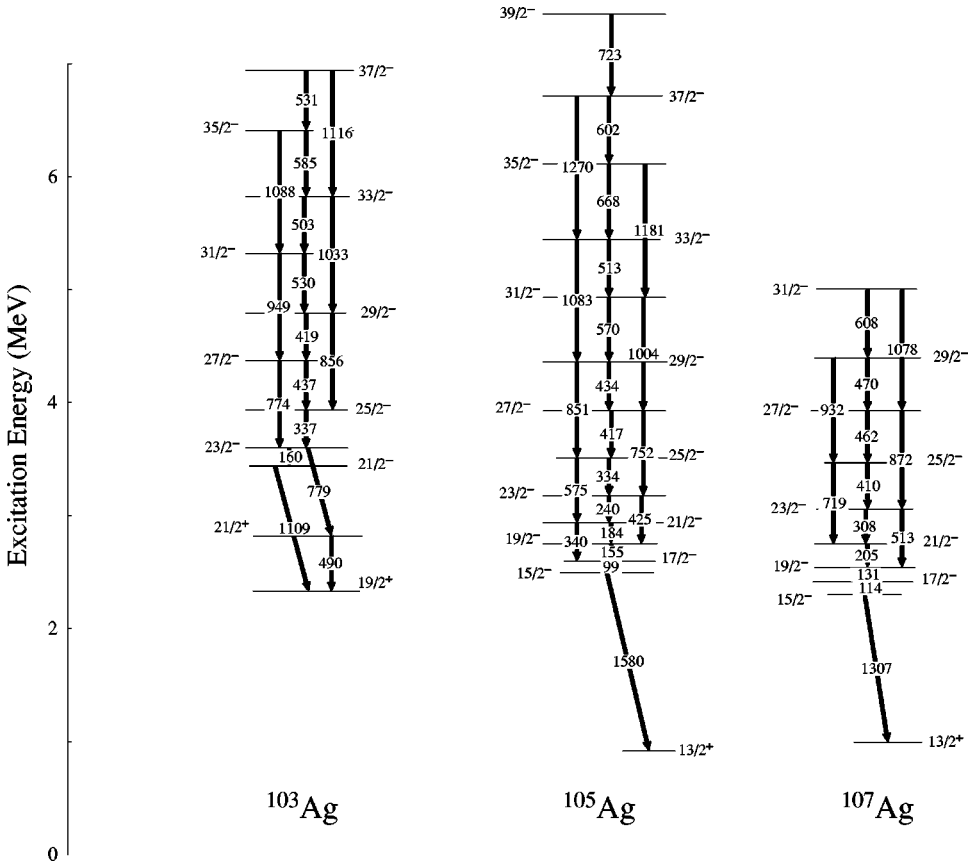

FIG. 8. The observed negative parity high spin bands in ^{103}Ag, ^{105}Ag [22], and ^{107}Ag [23], and their main feedout transitions.

parameters (ϵ_2, γ) [21] at $\hbar\omega = 0.3$ MeV and the values were found to be 0.13 and 28°, respectively.

The results of the TAC calculations are shown in Fig. 6 where the experimental and calculated level energies have been plotted as a function of total angular momentum. The calculated values were normalized to the experimental values at $I = 21/2\hbar$. It is observed from Fig. 6 that the calculations are able to reproduce the experimental slope reasonably well. This supports the choice of configuration and deformation values associated with the negative parity bands in ^{103}Ag.

The calculated values of $B(M1)/B(E2)$ ratios for $Q_0 = 1.5$ *e* b are shown in Fig. 4 by the solid line. It is seen from the figure that the magnitude of the $B(M1)/B(E2)$ ratios has been better reproduced by the TAC calculations as compared to the geometrical model. It is also to be noted that the calculated values lie between the observed values for bands 1 and 2. This is probably due to the fact that the TAC calculation was performed for the configuration $\pi g_{9/2} \otimes \nu(g_{7/2}d_{5/2})^1 \otimes \nu h_{11/2}$, which has admixtures from the two specific configurations for these bands, namely, $\pi g_{9/2} \otimes \nu d_{5/2} \otimes \nu h_{11/2}$ and $\pi g_{9/2} \otimes \nu g_{7/2} \otimes \nu h_{11/2}$. It, therefore, looks that the signature symmetry is required to explain the observed staggering, whereas the tilted axis rotation is needed to explain the experimental $B(M1)/B(E2)$ ratios for the negative parity bands in ^{103}Ag. These observations are understood by noting that the tilted minimum for ^{103}Ag is quite broad and shallow as seen from the plot of total quasiparticle Routhians as a function of the tilt angle (θ) for $\hbar\omega = 0.3$ in Fig. 7(a). This curve shows an energy difference of only 90 keV at 70° and 89°, thereby suggesting the possibility of a coexistence of the tilted and principal axis rotation with $\theta = 90°$.

In order to check this conjecture, the behavior of the negative parity bands in ^{105}Ag [22] and ^{107}Ag [23] have also been investigated. Figure 8 shows that the negative parity bands in ^{105}Ag and ^{107}Ag exhibit a regular increase in $M1$ transition energies with increasing spin upto $I = 31/2\hbar$, which is in contrast to the observed staggering in ^{103}Ag. The calculated equilibrium tilt angle and the corresponding deformation parameters at $\hbar\omega = 0.3$ MeV for $\pi g_{9/2} \otimes \nu(g_{7/2}d_{5/2})^1 \otimes \nu h_{11/2}$ configuration for ^{103,105,107}Ag are listed in Table III. The calculations were performed following the prescription given in Ref. [21]. It is seen from the table that all the three nuclei are predicted to be triaxial with increasing quadrupole deformation (ϵ_2) from ^{103}Ag to ^{107}Ag. The increase in ϵ_2 is due to the increased occupation of the $h_{11/2}$ orbital by the neutrons with increase in neutron number. The tilted minima for ^{105,107}Ag show an increase both in tilt angle and depth of the minima in the plots for total quasiparticle Routhians vs the tilt angle (Fig. 7). Thus, the energy difference of total

TABLE III. Deformation parameters and values of the equilibrium tilt for ^{103,105,107}Ag.

Nucleus	ϵ_2	γ	θ_0	$(e)_{\theta=89°} - (e)_{\theta=\theta_0}$ (keV)
^{103}Ag	0.13	28°	70°	90
^{105}Ag	0.19	24°	63°	180
^{107}Ag	0.24	20°	52°	320

quasiparticle Routhian at θ_0 and 89° increases substantially from ^{103}Ag to ^{107}Ag as shown in Table III. It, therefore, suggests that a small tilt angle and the shallow minimum allow a coexistence of principal and tilted axis rotation in ^{103}Ag, whereas larger tilt angle and deeper minima lead only to tilted axis rotation in ^{105,107}Ag.

V. CONCLUSIONS

The present experimental data have established the presence of nearly degenerate negative parity bands in ^{103}Ag, which exhibit staggering in $M1$ transition energies with opposite phases. The experimentally observed signature splitting has been used to assign the configurations (viz., $\pi g_{9/2} \otimes \nu d_{5/2} \otimes \nu h_{11/2}$ and $\pi g_{9/2} \otimes \nu g_{7/2} \otimes \nu h_{11/2}$) to bands 1 and 2, respectively. The $B(M1)/B(E2)$ ratios obtained from the geometrical model of Dönau and Frauendorf show higher values for band 1 compared to band 2 in agreement with the experimental observations. The calculated values are, however, larger than the experimental values for both the bands. On the other hand, $B(M1)/B(E2)$ values calculated using the TAC show better agreement and they lie between the experimental ratios for the two bands. This is indeed to be expected since the TAC calculations assume admixture of both the configurations. The signature symmetry for both the bands is, however, retained due to the fact that the tilted minimum for ^{103}Ag is shallow.

ACKNOWLEDGMENTS

The Clover array was set up at TIFR Pelletron jointly by TIFR, Mumbai; SINP, Kolkata; IUC-DAEF, Kolkata; and NSC, New Delhi. The authors would like to thank all the participants in this joint National effort. The authors would also like to thank Dr. S.D. Paul for his participation during the data collection and all the technical staff of Pelletron for smooth operation of the machine.

[1] Amita *et al.*, At. Data Nucl. Data Tables **74**, 283 (2000); see www.nndc.bnl.gov/nndc/mag-dip-rot-bands/
[2] S. Frauendorf, Rev. Mod. Phys. **73**, 463 (2001); Nucl. Phys. **A557**, 259c (1993).
[3] R.M. Clark *et al.*, Phys. Rev. Lett. **82**, 3220 (1999).
[4] J. Persson *et al.*, Nucl. Phys. **A627**, 101 (1997).
[5] D.G. Jenkins *et al.*, nucl-ex/0007004.
[6] D.G. Jenkins *et al.*, Phys. Lett. B **428**, 23 (1998).
[7] J. Treherne *et al.*, Nucl. Phys. **A342**, 357 (1980).
[8] M. Saha Sarkar *et al.*, Nucl. Instrum Methods Phys. Res. A **A491**, 113 (2002).
[9] D.C. Radford, Nucl. Instrum. Methods Phys. Res. A **361**, 297 (1995); **361**, 306 (1995).
[10] M. Meyer *et al.*, Nucl. Phys. **A316**, 93 (1979).
[11] B. Crowell *et al.*, Phys. Rev. C **45**, 1564 (1992).
[12] I. Hamamoto, Phys. Lett. B **235**, 221 (1990).
[13] E. Galindo *et al.*, Phys. Rev. C **64**, 034304 (2001).
[14] F. Dönau, Nucl. Phys. **A471**, 469 (1987).
[15] P.H. Regan *et al.*, Nucl. Phys. **A586**, 351 (1995).
[16] T. Lonnröth *et al.*, Z. Phys. A **317**, 215 (1984).
[17] F. Dönau and S. Frauendorf, in *Proceedings of the International Conference on High Angular Momentum Properties of Nuclei*, Oak Ridge, 1982, edited by N. R. Johnson (Harwood, New York, 1983), p. 143.
[18] V.I. Dimitrov, S. Frauendorf, and F. Dönau, Phys. Rev. C **62**, 024315 (2000).
[19] A.H. Wapstra and G. Audi, Nucl. Phys. **A595**, 409 (1995).
[20] R. Bengtsson, S. Frauendorf, and F.R. May, At. Data Nucl. Data Tables **35**, 15 (1986).
[21] Amita *et al.*, Phys. Rev. C **64**, 034308 (2001).
[22] Dan Jerrestam *et al.*, Phys. Rev. C **52**, 2448 (1995).
[23] F.R. Espinoza-Quinones *et al.*, Phys. Rev. C **55**, 1548 (1997).